CELLULOSE NANOFIBER FROM YERBA MATE STICKS: SURVEY OF MORPHOLOGICAL, CHEMICAL AND THERMAL PROPERTIES

RUAN EZEQUIEL GEMMER,[*] CLEIDE BORSOI,[*] BETINA HANSEN,[*]
EDSON LUIZ FRANCISQUETTI,[**] HEITOR LUIZ ORNAGHI JR.,[***]
ADEMIR JOSÉ ZATTERA[****] and ANDRÉ LUIS CATTO[*]

[*]*Ciências Exatas e Engenharia, Universidade do Vale do Taquari - Univates, Lajeado, RS, Brazil*
[**]*Instituto Federal de Educação, Ciência e Tecnologia do Rio Grande do Sul - IFRS, Farroupilha, RS, Brazil*
[***]*Mantova Indústria de Tubos Plásticos Ltda., R. Isidoro Fadanelli, 194, Centenário, Caxias do Sul, RS, Brazil*
[****]*Universidade de Caxias do Sul - UCS, Programa de Pós-Graduação em Engenharia de Processos e Tecnologias (PGEPROTEC), Caxias do Sul, RS, Brazil*
✉ *Corresponding author: C. Borsoi, eng.cleide@yahoo.com.br*

Received July 11, 2023

This study aims to evaluate different process conditions for obtaining cellulose nanofibers (CNFs) from yerba mate residues. This includes chemical (bleaching and/or TEMPO-oxidation), physical (steam explosion), and mechanical treatments (ultrafine grinding). All treatments demonstrated to be efficient in obtaining CNFs, as observed from a morphological analysis by transmission electronic microscopy (TEM). A reduction of hemicelluloses and an increase in cellulose content was observed from the Fourier-transform infrared spectroscopy (FTIR) results, after all the treatments. The yerba mate sample that underwent physical/chemical/mechanical treatments showed a higher thermal degradation temperature peak at 333 °C, with a degradation of 50% of the initial mass. The activation energy (E_a) increased from 33% to 64%, when the CNFs were obtained using the derivative Friedman method for all the samples, and this method presented a greater proximity to the experimental results. These results demonstrate that CNFs can be obtained from yerba mate residues, to valorize this lignocellulosic biomass.

Keywords: cellulose nanofiber, yerba mate, residues

INTRODUCTION

Agricultural residues from different sources have been widely studied for isolation of nanocellulose.[1–3] According to Dahlem Jr *et al*.,[4] yerba mate (YM) stick particles are a prominent raw material for nanocellulose extraction. YM has a high utilization in South America (especially in Brazil, Paraguay, and Argentina) mainly attributed to the consumption of a yerba mate based drink with hot water, served in a gourd and ingested using a metal straw called "chimarrão".[4,5] The huge consumption leads to large amounts of residues, as YM stick particles correspond to approximately 2% of its mass production.[6,7] These residues are mainly composed of 34.85% α-cellulose, 24.77% hemicelluloses, 25.78% lignin, 10.11% extractives, and 4.49% ash,[6] which makes this material suitable for nanocellulose extraction and would generate a final high value-added product.

Nanocellulose is a prominent material[1] and can be classified based on its morphology into: i) nanofibrils (*i.e*., cellulose nanofibers (CNFs)), ii) nanocrystals (CNCs), or iii) bacterial nanocellulose.[2] Nanocellulose has several characteristics, such as biodegradability, biocompatibility, nontoxicity, greater surface area, higher crystallinity and mechanical strength, high elasticity modulus, easy surface functionalization, and high chemical resistance. This allows their use in several fields, including biomedical, pharmaceutical, aerospace, automobile, food packaging, and green nanocomposite materials.[1,8] The low cost and renewability are also positive aspects.[9] The

incorporation of small amounts of CNCs or CNFs can enhance the mechanical, thermal, and barrier properties of the polymer, in addition to providing lightweight materials compared to conventional composites.[9,10] To evaluate the potential application of nanocellulose as a reinforcing agent in composites and to determine the process parameters, the thermal behavior of nanocellulose is a crucial parameter to be studied.[11] It is known that the residues of the hemicelluloses and lignin, as well as the type and content of the surface groups generated in different manufacturing processes have influence on the thermal behavior of nanocellulose.[12]

The final properties of nanocellulose depend on the extraction process, the source material, and the pre- or post-treatment.[1,2] Therefore, the technique for isolating the nanocellulose from different sources is crucial and must be considered to efficiently exploit these resources. After the pretreatment, various physical, mechanical, or chemo-mechanical treatments can be used to isolate CNFs from cellulosic fibers, including high-pressure homogenization, high-intensity ultrasonication, electrospinning, grinding, and steam explosion.[10,13] According to Trache *et al*.,[1] a combination of these processes can be an interesting approach, as it can overcome some of the shortcomings of a single method. Acid and enzymatic hydrolyses are the most used techniques for obtaining CNCs, whereas CNFs require strong mechanical machinery to be produced. This mechanical machinery presents some limitations, such as high energy consumption and size reduction of the raw material. To minimize these drawbacks, several pretreatments have been studied.[10,13] The pretreatments include bleaching, acid hydrolysis, enzyme hydrolysis, and TEMPO-mediated oxidation (using 2,2,6,6-tetramethylpipelidine-1-oxyl radical).[13,14] After the pretreatment, various physical, mechanical, or chemo-mechanical treatments can be used to isolate CNFs from cellulosic fibers, including high-pressure homogenization, high-intensity ultrasonication, electrospinning, grinding, and steam explosion.[10,13]

In this work, CNFs were obtained from YM residues using different processes, such as bleaching, TEMPO oxidation, steam explosion, and ultrafine grinding. For each treatment, the thermal, chemical, and morphological properties of the obtained CNFs were evaluated. Also, the thermal degradation kinetics was evaluated, and the kinetic parameters were discussed. This study has the potential to increase the applicability of nanocellulose as reinforcement in composites based on different polymer matrices, besides its sustainability and environmental appeal due to the incorporation of a large amount of YM sticks into composites. Finally, YM residues are an important type of biomass that has great potential to be used for new applications.

EXPERIMENTAL

Materials

YM residue was obtained from the Elacy Co. (Venâncio Aires city, Brazil) in the form of ground sticks. Sodium hydroxide (NaOH, 98%), ammonium ferrous sulfate (98.5%), sulfuric acid (H_2SO_4, 97%), hydrochloric acid (HCl, 37%), potassium dichromate (99%), hydrogen peroxide (H_2O_2, 33%), sodium hypochlorite (NaClO, 12%), sodium bromide (NaBr, 98%) were obtained from LabSynth (São Paulo, Brazil). Acetone (99.5%) and TEMPO (98%) reagents were purchased from Sigma Aldrich (Barueri, Brazil). All reagents were used as received.

Isolation of cellulose nanofibers

YM sticks were ground in a knife mill and sieved to obtain particles smaller than 150 Tyler mesh size (106 μm). The fibers were subjected to different treatments, including physical-chemical (steam explosion), chemical (bleaching and/or TEMPO-mediated oxidation), and mechanical (ultrafine friction grinding) methods. The nomenclature of the samples is shown in Table 1.

Steam explosion process

The steam explosion process was applied to YM/PC and YM/PCM samples using a methodology similar to that performed by Dahlem Jr. *et al*.[4] A mixture of YM fibers and water (1:10 wt.) was treated in an autoclave (Phoenix Luferco AV, Brazil) at 130 °C and 166.7 kPa, with four steam explosion sequences. The first explosion was performed 30 min after the equipment reached the aforementioned conditions. The other three explosions were performed after 10 min of stabilization of the autoclave. The fibers were washed three times with water, and centrifuged at 1600× g.

Bleaching process

Bleaching was performed in two stages using a method adapted from the literature.[15,16] The first step was treatment with an NaClO solution (7.5% v/v) in a ratio of 1:10 wt. (fiber:water) for 60 min at 60 °C using a vapor condensation system. Posteriorly, bleaching was performed with an H_2O_2 solution (10% v/v), under the same conditions of the first step. At the end of each bleaching step, the fibers were washed three times with water and centrifuged at 1600× g.

TEMPO-mediated oxidation process

TEMPO-mediated oxidation was performed using a 1 wt% suspension of fibers in water, with 0.016 g TEMPO, 0.1 g NaBr, and 10 mmol NaClO per initial gram of sample, in a system with soft stirring at 25 °C. The pH was maintained constant at 10, with a 0.5 M NaOH solution, and the reaction proceeded for approximately 60 min.[17,18] The oxidized cellulose was filtered through a filter glass crucible (70 µm porosity), washed twice in water at 4 °C, and purified to give a 2.0 wt% suspension, centrifuged at 3500× g for 30 min, before being stored in a refrigerator at 4 °C.

Table 1
Nomenclature of samples and treatment methods performed

Sample	Treatment process		
YM	-	-	-
YM/PC	Steam explosion	Bleaching	TEMPO
YM/PCM	Steam explosion	Bleaching	Ultrafine grinding
YM/CM	Bleaching	TEMPO	Ultrafine grinding

P = physical process, C = chemical process, M = mechanical process

Ultra-fine friction grinding process

Ultrafine grinding was performed (Masuko Sangyo Supermasscolloider MKCA6-2, Japan) as the final step to obtain CNFs. The samples had a solid concentration of 2 wt% in an aqueous solution. A total of 50 passes were made in the mill at 1500 rpm (central electrical control box) and the final suspension was refrigerated at 4 °C.

Characterization

Scanning electron microscope (SEM)

The morphological characterizations were carried out in a scanning electron microscope (SEM) (Carl Zeiss EVO-LS10, Germany), at an accelerating voltage of 10 kV and magnification of 500x. The samples were coated with a thin layer of gold.

Transmission electronic microscopy (TEM)

The samples were sonicated for 10 min prior to deposition on a thin carbon-coated microgrid, and subsequently stained with a uranyl acetate solution (2 wt%). The morphologies of the cellulose nanofibers were analyzed using a transmission electron microscope (TEM, FEI Tecnai G2 T20, United States) at a voltage of 80 kV and magnification of 39000x.

Fourier-transform infrared spectroscopy (FTIR)

The FTIR spectra were obtained using an infrared spectrophotometer (Perkin Elmer Frontier, USA) with an attenuated total reflectance accessory (ATR). The wavelength range used was between 400 and 4000 cm^{-1}, and each spectrum was recorded using 32 scans.

X-ray diffraction (XRD)

An X-ray diffractometer (Bruker Siemens D-5000, Germany) was used to perform X-ray diffraction analysis. A voltage of 40 kV and current of 30 mA were used, with a monochromatic beam of Cu Kα radiation (λ = 0.154 nm), in a reading range between 5° and 40° (2θ) with a velocity of 0.02°/2 s. The calculation of the crystallinity index was done according to Equation 1:

$$\textbf{Crystallinity index} = \frac{\textbf{area from 16 to 24}}{\textit{entire curve}} \text{ x } 100 \quad (1)$$

Thermogravimetric analysis (TGA)

Initially, the samples were oven-dried with air circulation for 24 h at 60 °C prior to thermogravimetric analysis. The tests were performed using a thermogravimetric analyzer (Shimadzu TGA-50, Japan) at a heating rate of 10 $°C.min^{-1}$, nitrogen flow rate of 20 $mL.min^{-1}$, in the temperature range of 25 to 800 °C.

Kinetic study

The thermal degradation kinetic study was performed to evaluate the effect of different treatments on the activation energies, pre-exponential factors and reaction mechanism. Three curves at different heating rates were used (10, 20, and 40 °C/min for each sample), and isoconversional kinetic methods were considered.[11,12,19,20]

The estimation of the conversion degree (α) was calculated considering the initial mass (m_0), mass at temperature/time T (m), and final mass (m_f) according to Equation 2, as follows:

$$\alpha = \frac{m_0 - m}{m_0 - m_f} \quad (2)$$

The reaction rate (dα/dt) considers the rate constant k(T) (which follows the Arrhenius equation); the reaction model f(α) is a function of the conversion, and is represented by Equations 3 and 4 as follows:

$$\frac{d\alpha}{dt} = k(T)f(\alpha) \quad (3)$$

$$k(T) = Ae^{\frac{-Ea}{RT}} \quad (4)$$

In the above, A is the pre-exponential factor (min^{-1}), Ea is the activation energy ($kJ.mol^{-1}$), R is the gas constant (8.314 $J.mol^{-1}K^{-1}$), and T is the absolute temperature (K). By combining Equations 3 and 4, Equation 5 can be obtained. When the heating rate β = dT/dt, the equation can be rewritten as Equation 6:

$$\frac{d\alpha}{dt} = A\left[\exp\left(\frac{-Ea}{RT}\right)\right]f(\alpha) \quad (5)$$

$$\frac{d\alpha}{dt} = \left(\frac{A}{\beta}\right)A\left[\exp\left(\frac{-Ea}{RT}\right)\right]f(\alpha) \quad (6)$$

Two different methods were chosen for comparison: i) the integral Flynn-Wall- Ozawa (FWO) method, and ii) differential Friedman method. The activation energy and pre-exponential values were discussed and compared.

The FWO method considers the heating rate β, and introduces g(α) as a function of the conversion. The FWO equation is expressed according to Equation 7 as follows:

$$Log\beta = \log\left[\frac{AE_a}{g(\alpha)R}\right] - 2.315 - 0.4567\frac{E_a}{RT} \quad (7)$$

The activation energy is obtained from the slope ($0.4567\frac{E_a}{R}$) for the log β versus 1/T plot.

The Friedman method considers that the decomposition of the conversion function f(α) depends only on the rate of the mass loss, as described by Equation 8 as follows:

$$Ln\left(\frac{d\alpha}{dt}\right) = \ln[Af(\alpha)] - \frac{E_a}{RT} \quad (8)$$

The activation energy ($-\frac{E_a}{R}$) can be obtained from the slope of $Ln\left(\frac{d\alpha}{dt}\right)$ against 1/T plot.

If the reaction model f(α) is expressed in a more analytical way, Equation 8 can be obtained. In Equation 9, m, n and p are constants, and their combination represents the suggested reaction model,[21,22] as shown in Table 2.

$$f(\alpha) = \alpha^m(1-\alpha)^n[-\ln(1-\alpha)]^p \quad (9)$$

Equation 8 was used with the help of the software developed by Drozin *et al.*,[23] Briefly, Vyazovkin and FWO methods were compared, and the activation energies and pre-exponential values were obtained for both methods. The mechanism function was not limited to a set of models. The relative error, when compared to both methods, is indicative of a single- or multi-stage process. Values lower than 10% are indicative of a single-step process, while values higher than 10% indicate a multi-step process.

Table 2
Combination of m, n, and p constants for the respective reaction models

Combination of			Reaction model
m	n	p	
●	●	●	Phase boundary reaction
●	X	●	Phase boundary reaction (unimolecular decay law)
X	●	●	Nucleation, linear growth of nuclei, linear diffusion
●	●	X	Diffusion
X	X	●	Nucleation, latte stages of linear growth of nuclei
●	X	X	Growth of nuclei
X	●	X	Unjustified as yet
X	X	X	Any complicated case, unjustified as yet

Adapted from[21]

RESULTS AND DISCUSSION

Morphological analysis

The TEM and SEM micrographs of the samples are shown in Figure 1. Figure 1 (a-c) shows the TEM micrographs of the samples after the treatments, whereas Figure 1 (d) shows the SEM micrograph of the YM sample without treatment. It can be observed (Fig. 1 (d)) that the YM fibers used in the treatment are of different sizes. In addition, it is possible to identify the presence of monoclinic crystals (red arrows). According to our previous work,[24] these crystals are calcium oxalate, which is present with varied morphologies and concentrations in plants and are derived from the cultivated soil.[25]

The TEM micrographs show that CNFs were successfully obtained from the YM fibers after all the treatments. The obtained nanofibers have a diameter of approximately 10 nm, but their length is much higher, resulting in a large fiber length and diameter (L/D) aspect ratio. This is corroborated by literature, which defines a diameter range from 1 to 100 nm for CNFs.[26] Similar results were obtained by Dahlem Jr. *et al.*,[4] where the authors obtain nanocellulose from YM through physical and chemical treatments. It can also be observed in Figure 1 (b) that the YM/PCM sample has a larger diameter relative to the other samples, which may be related to the absence of TEMPO oxidation. According to Kaffashsaie *et al.*,[26] the use of the TEMPO oxidation process is related to the isolation of nanocellulose due to the high electrostatic forces caused by the oxidation between the elementary fibrils, resulting in greater fibrillation.

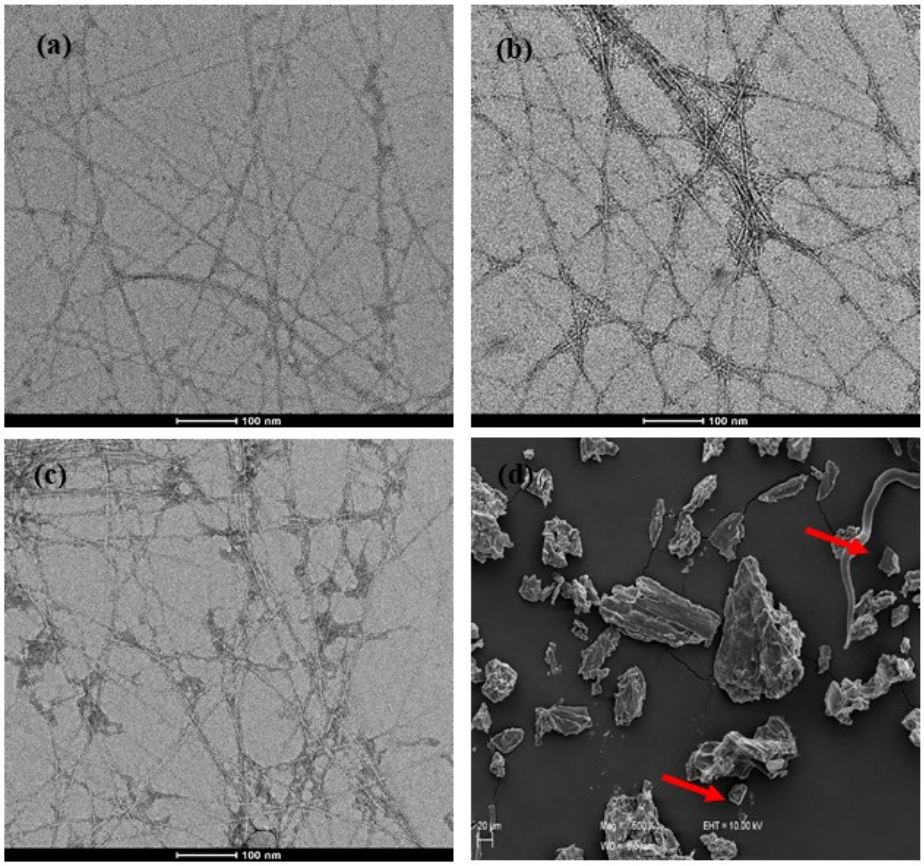

Figure 1: TEM micrographs of YM/PC (a), YM/PCM (b), YM/CM (c) and SEM image of YM (d)

FTIR analysis

FTIR spectroscopy (Fig. 2) was used to verify changes in the chemical composition of the YM fibers after treatment. The peak at 1735 cm^{-1} can be attributed to the C=O bonds of the acetyl groups and esters present in hemicelluloses.[27,28] Peak displacements from 1600 to 1620 cm^{-1} can be observed in the samples YM/PC and YM/CM, relative to YM and YM/PCM. This can be explained by the formation of carboxylate groups owing to the oxidative treatment with the TEMPO process.[29,30]

The peak at 1515 cm^{-1} is attributed to the C=C bonds,[27,31,32] while the region at 1240 cm^{-1} is assigned to the C-O or C-O-C bonds, both present in lignin.[31,33–35] No peak is observed at 1515 cm^{-1} for YM/PC and YM/PCM, while a low intensity peak is observed for YM/CM. The peak in the 1200–1280 cm^{-1} range showed a reduced intensity for YM/PC and YM/PCM, possibly attributed to the severe condition of the steam explosion treatment for the delignification of the crude material.

A decrease in the hemicellulose content is suggested by the reduction in the peak intensity at 1370 cm^{-1} corresponding to the stretching vibration of the C-H bonds.[36] The increase in the peak at 896 cm^{-1} for the treated samples is characteristic of an increase of the C-O-C vibrations in the form of the β-(1–4)-glycosidic bonds of cellulose.[32] This increase in cellulose content has also been reported by other researchers.[27,37,38]

The absorbance peak intensities at 1317 and 781 cm^{-1} increase after treatment in relation to YM. Such vibrations may be attributed to the presence of the crystalline material that was already present in the initial sample. The literature cites similar peaks in the FTIR spectra of plants naturally containing calcium oxalate.[39,40]

Other possible changes were calculated using the different ratios between some specific bands. Since possible changes in the crystallinity index are expected in different fibers depending on the process, the band characteristics of the two crystalline cellulose allomorphs occur at approximately 3300 cm^{-1}. The two crystalline allomorphs are cellulose I_α and cellulose I_β. Hence, the hydrogen bonds present only in cellulose can be indirectly estimated using the energy of the hydrogen bonds (E_H) (Eq. 10) and the hydrogen bond distances (R) (Eq. 11):[41]

$$E_H = \frac{1}{k}\frac{v_0 - v}{v_0} \quad (10)$$

$$\Delta v(cm^{-1}) = 4430 \times (2.84 - R) \quad (11)$$

where v_0 is the standard frequency corresponding to free OH groups; v is the frequency of the bonded OH groups; k is a constant (1/k = 262.5 kJ), $\Delta v = v_0 - v$ (v_0 is the monomeric OH stretching frequency (at 3600 cm^{-1})) and v is the stretching frequency observed in the FTIR spectrum.

Also, the band around 1425 cm^{-1} is associated with the amount of the crystalline structure of the cellulose, while the band at 898 cm^{-1} is assigned to the amorphous region in cellulose. The ratio between the bands is associated with an empirical crystallinity index (LOI). Another ratio (TCI) (1370 and 2900 cm^{-1}) is also used to estimate another crystallinity index. The results are presented in Table 3.

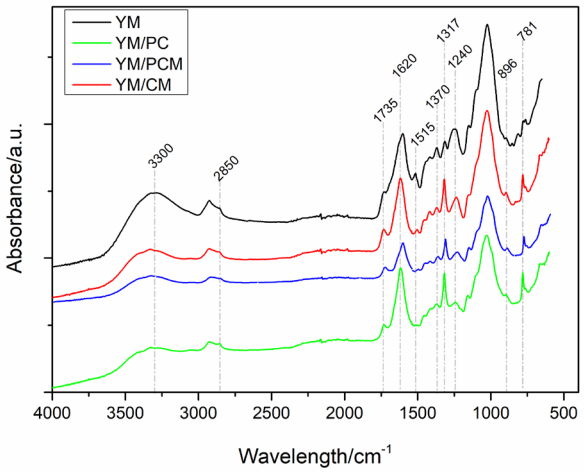

Figure 2: FTIR spectra of YM and treated samples

Table 3
Energy of hydrogen bonds, hydrogen bond distance, and infrared crystallinity ratio using two different approaches

Sample	E_H (kJ)	R (Å)	LOI	TCI
YM	21.51	2.91	1.74	0.39
YM/PC	20.27	2.90	1.62	0.35
YM/PCM	19.54	2.90	1.58	0.35
YM/CM	18.88	2.90	1.58	0.35

The energy of the hydrogen bonds decreases with the treatment, while the hydrogen bond distance seems not to be affected. Both crystallinity indices estimated by FTIR also presented higher values for YM compared to all other treated samples. It is noteworthy that the parameters calculated consider only the crystalline cellulose portion of the fiber and not ordered portions of hemicelluloses, for example. It is also important to mention that cellulose can contain a wide variety of amorphous content, which may as well influence the crystal size, cellulose polymorph, and the degree of polymorphic conversion.[42] Another crucial point is that the data obtained above consider only a single numerical point, and not any changes in band intensity. Despite all these drawbacks, these variables seem to be valuable for comparison, in corroboration with other techniques.

The results from Table 3 are presented in relation to the Kendall correlation type to visualize some eventual correlation among the variables (Fig. 3). The correlation coefficient is presented inside the ellipses. It is noted that a negative correlation (observed by the red ellipses) is present for all variables, there being a higher correlation between E_H and LOI. Lower correlations were among the variables E_H and R and TCI and E_H. This indicates that the energy of the hydrogen bonds has a strong influence on the variables from FTIR. It is important to remember that these parameters are estimated considering the cellulose portions of the FTIR spectra. In this sense, the cellulose content when estimated by

LOI (1425/898 ratio) seems to decrease the crystallinity content by weakening the energy bond between the hydrogen bonds. However, if the TCI is considered, a weaker correlation is observed, which has not a direct influence on the crystallinity index.

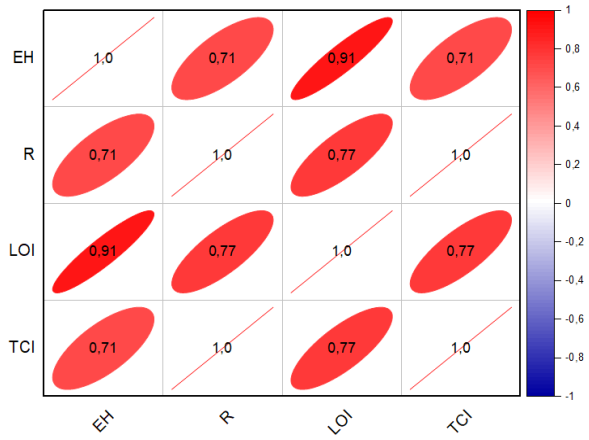

Figure 3: Correlation plot among the variables obtained by FTIR

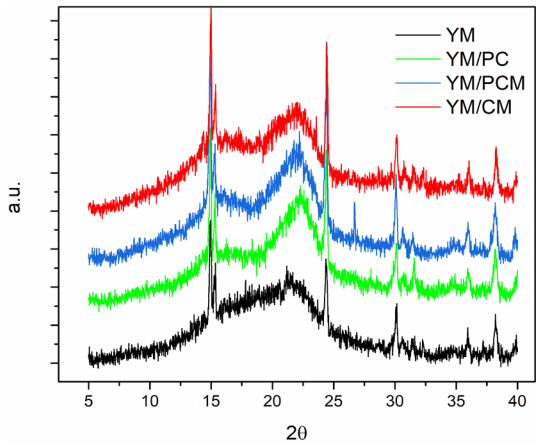

Figure 4: XRD spectra of differently treated YM fibers

XRD analysis

XRD spectra (Fig. 4) were used to verify the influence of the treatment on the crystallinity index. In our earlier study,[24] the results showed an increase in the crystallinity index of up to 23% using the steam explosion treatment as the first step of the treatment (for YM/PC and YM/PCM). Differently from the previous work, where data smoothing was applied, in the present study, raw data were used to estimate the crystallinity.

The curves of the treated samples are very similar, with a more defined amorphous halo between the crystalline peaks at 2θ from 16 to 24. The crystallinity values were 33.14, 34.42, 33.41, and 28.08 for YM, YM/PC, YM/PCM, and YM/CM, respectively. This indicates that the crystallinity portion of the samples was not significantly altered (if any) by the treatment. The results somehow corroborate with the FTIR findings.

Thermal degradation

The thermal degradation behavior of the studied samples is shown in Figure 5. For all samples, an initial mass loss lower than 5% between 60 and 150 °C is observed. This mass loss may be related to the evaporation of water molecules, or to the presence of other low molecular weight volatile substances as waves from the sample surface.[2,43] The YM sample shows a higher thermal degradation loss between 150 and 350 °C, with a 51% mass loss in this temperature range, and a final residue of 27% mass at 750 °C in a nitrogen atmosphere. A similar result was obtained by Hugen *et al.*[32] when evaluating the incorporation of carboxylated styrene-butadiene rubber in composite films of cellulose nanofibrils obtained from *Eucalyptus* sp. kraft pulp.

For the treated samples (Fig. 5a), the curves extended to higher temperatures, compared to YM, prior to significant thermal degradation between 150 and 200 °C. This may be attributed to the lower concentration of hemicelluloses in the treated samples. Hemicelluloses begin degrading at approximately 200 °C, while cellulose begins degrading near 300 °C.[44] A decrease in the maximum thermal degradation temperature (observed by the DTG peak) is observed in the YM/PC and YM/CM samples, relative to that in YM (Fig. 5b). Similar results were reported in the literature[45,46] for TEMPO-mediated oxidation samples, and were attributed to the dissociation of the intermolecular hydrogen bonds by introducing carboxyl groups on the surfaces of the cellulose fibers.

YM/PCM showed higher thermal stability (9% higher compared to YM) and thermal degradation temperature peak (333 °C with a degradation of 50% of the initial mass), compared to the other samples. This increase in the thermal degradation temperature is related to a combination of higher cellulose concentration (which decomposes mainly between 300–370 °C),[27,47] higher crystallinity, and lower lignin and hemicellulose content.[2] Similar results were reported

elsewhere.[2,43,48] Other peaks are observed at 450 °C and 650 °C (Fig. 5b) for all the samples, possibly representing the disruption of the β-O-4 bonds and a secondary pyrolysis reaction of the lignin, respectively.[44]

Kinetic study

A kinetic analysis of the different CNFs was performed using the FWO and Friedman methods. For the FWO method, it was assumed that the reaction order was close to 1, whereas for the Friedman method, any assumptions for the order of reaction were performed directly using the mass conversion from the TGA.[49] The thermal stability of natural fibers is of great industrial and academic importance, as degradation can occur at different rates depending on the type of sample, geometry, chemical composition, etc.[11,50]

Figure 6 represents the plots of log β or ln(dα/dt) versus 1/T for both methods, from each conversion in the range (0.2–0.8) for the different samples. The degree of conversion for 0.2–0.8 is presented because it represents a more important conversion range for the degradation step (degradation of the cellulose component), corresponding to 60% or more of the fiber.[50] In general, a similar behavior of E_a is observed in relation to α conversion for both methods – an increase in the activation energy with the conversion degree. A similar trend can be found in the literature for coconut,[51] tobacco,[19] and grape stalk residues.[52]

Table 4 shows the kinetic parameters of the activation energy (E_a), coefficient of determination (R^2), and pre-exponential factor (ln A), as analyzed by both kinetic methods (FWO and Friedman) for different α. As can be seen in Table 4, the R^2 for the Friedman method presented values close to 1, indicating greater proximity to the experimental results. According to Ahuja *et al.*,[49] this difference can be explained based on the different calculation methods involved. According to Xu *et al.*,[53] the closer the R^2 is to 1, the better the adjustment effect used in the linearization of the curves. Thus, it is observed that the Friedman method presents the best R^2, as defined in Figure 6, and the dispersion points are distributed almost in a straight line of fit. This indicates that the results provided by the Friedman kinetic model are in agreement with the experimental results; accordingly, they exhibit a higher R^2 value.

The activation energy averages are 69.7 ± 13.9 kJ.mol^{-1}, 112.4 ± 53.1 kJ.mol^{-1}, 89.4 ± 14.1 kJ.mol^{-1}, and 105.7 ± 36.5 kJ.mol^{-1} for YM, YM/PC, YM/PCM, and YM/CM, respectively, for the FWO method. The E_a averages are 99.6 ± 18.2 kJ.mol^{-1}, 164.7 ± 60.5 kJ.mol^{-1}, 133.6 ± 30.5 kJ.mol^{-1}, and 150.4 ± 53.4 kJ.mol^{-1} for YM, YM/PC, YM/PCM, and YM/CM, respectively, for the Friedman method. Thus, higher values are observed for the YM/PC sample, indicating that the CNFs have higher activation energy than the pure sample (YM). This is indicative of a greater amount of energy required to start thermal decomposition.[31,49,53]

The average E_a increases by 33–64% for CNFs using the Friedman method. E_a is related to the amount of energy required to rupture the bonds between molecules.[49] A study carried out by Ornaghi Jr. *et al.*[50] observed that the main lignocellulosic components of the fibers have the following E_a values: cellulose: 157 kJ.mol^{-1}, hemicelluloses 110 kJ.mol^{-1}, and lignin 80 kJ.mol^{-1}. Hence, the reduction in the hemicelluloses, lignin, extractives, and other components that have lower thermal stability helps increase the thermal stability of the material.

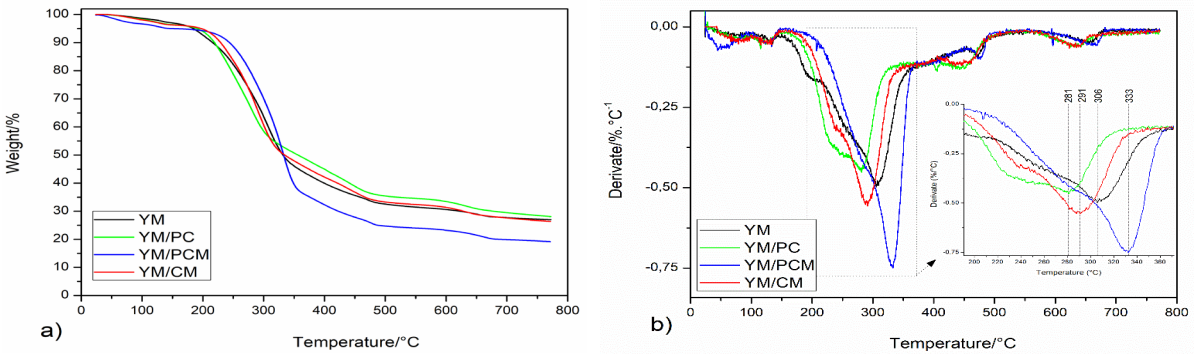

Figure 5: Thermal behaviors of YM and treated samples: (a) thermogravimetric (TG) and (b) derivative TG (DTG) curves

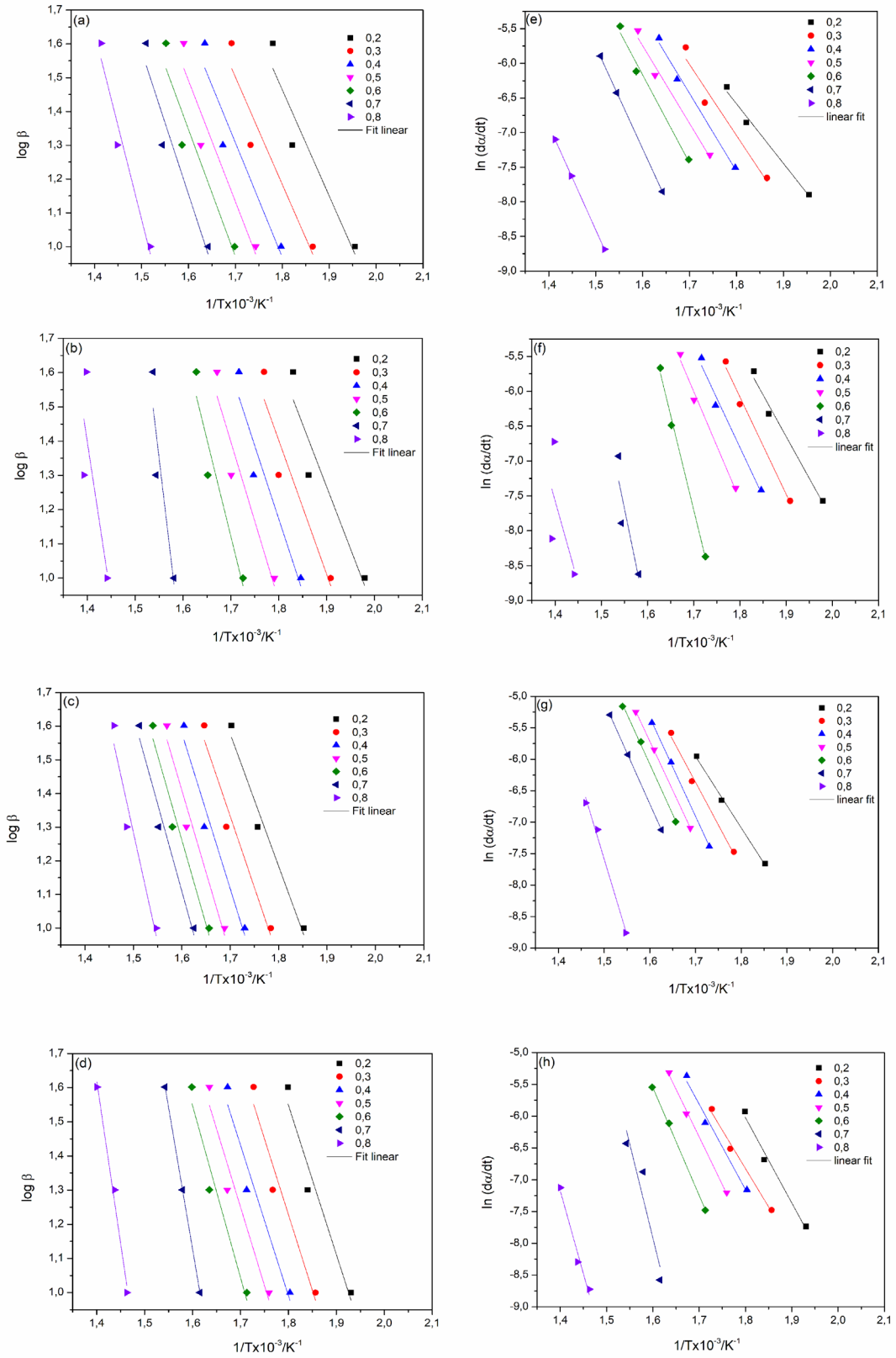

Figure 6: Kinetic plot for α = 0.2–0.8 using the Flynn-Wall-Ozawa (FWO) method for: (a) YM, (b) YM/PC, (c) YM/PCM and (d) YM/CM. Kinetic plot using the Friedman method for: (e) YM, (f) YM/PC, (g) YM/PCM and (h) YM/CM

Table 4
Summary of kinetic parameters for alpha conversion range of 0.2–0.8 by Flynn-Wall-Ozawa (FWO) and Friedman methods

α	YM			YM/PC			YM/PCM			YM/CM		
	Ea/kJ.mol^{-1}	ln A/min^{-1}	R^2	Ea/kJ.mol^{-1}	ln A/min^{-1}	R^2	Ea/kJ.mol^{-1}	ln A/min^{-1}	R^2	Ea/kJ.mol^{-1}	ln A/min^{-1}	R^2
FWO												
0.2	57.22	7.13	0.8295	66.22	8.18	0.8053	71.43	8.25	0.9509	79.63	9.43	0.9103
0.3	57.81	6.90	0.8272	71.19	8.45	0.8074	76.93	8.52	0.9267	80.81	9.22	0.9074
0.4	61.67	7.07	0.8314	77.58	8.85	0.8299	84.20	8.99	0.9303	80.12	8.92	0.9028
0.5	65.29	7.23	0.8307	84.18	9.26	0.8416	88.78	9.22	0.9319	83.48	9.05	0.8988
0.6	68.47	7.37	0.8278	103.28	10.77	0.8416	91.57	9.32	0.9391	91.52	9.59	0.9149
0.7	77.06	7.93	0.8588	215.77	19.73	0.7043	94.37	9.41	0.9423	150.89	14.40	0.9999
0.8	100.26	9.35	0.9250	168.41	14.36	0.3336	118.70	11.07	0.8977	173.70	14.99	0.9780
Friedman												
0.2	71.60	8.92	0.9794	99.48	16.08595	0.9704	94.24	13.31	0.9942	111.60	18.14	0.9716
0.3	84.99	11.36	0.9131	115.88	19.00887	0.9822	112.81	16.70	0.9858	100.30	14.89	0.9822
0.4	93.19	12.62	0.9846	117.11	18.5526	0.9649	130.65	19.80	0.9994	111.51	16.99	0.9703
0.5	93.29	12.21	0.9648	129.31	20.43797	0.9777	129.16	19.14	0.9996	124.65	19.16	0.9954
0.6	105.87	14.21	0.9745	226.02	38.514	0.9923	132.42	19.40	0.9962	141.04	21.59	0.9986
0.7	122.84	16.41	0.9997	268.02	42.28916	0.5832	134.93	19.25	0.9999	246.38	39.49	0.8000
0.8	125.37	14.21	0.9999	196.75	25.56394	-0.1831	200.83	28.64	0.9803	216.98	29.36	0.9519

Ornaghi Jr. *et al.*[50] and Zhang *et al.*[31] demonstrated that lignin (an amorphous compound) has lower activation energy, and hence requires lower energy to start the degradation process (on the other hand, a small portion of lignin degrades at higher temperatures).

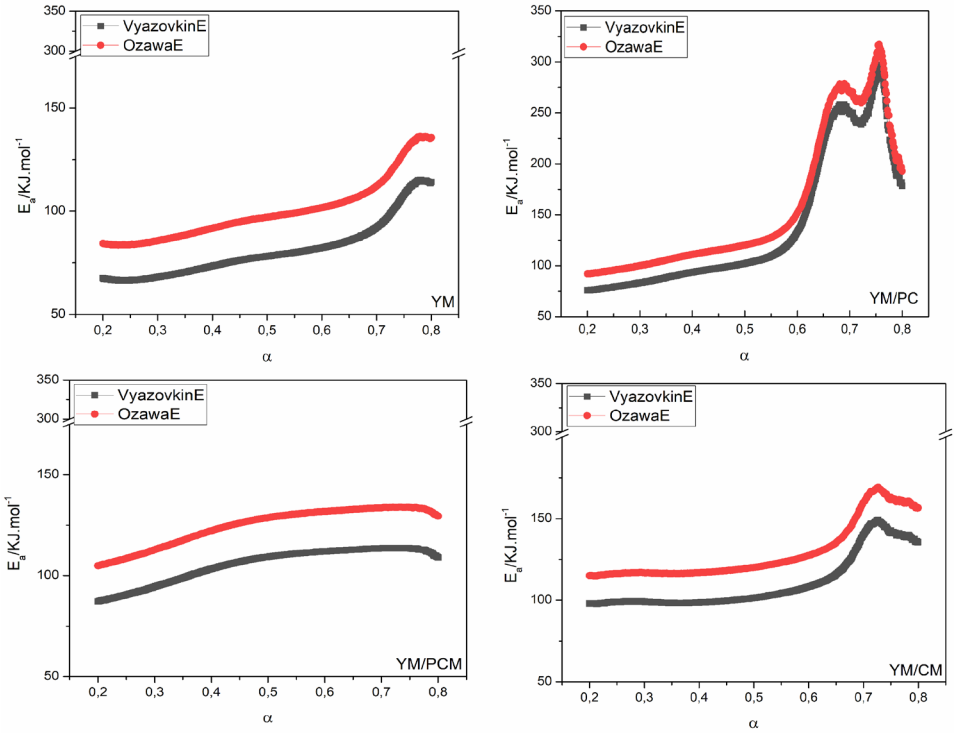

Figure 7: Activation energy as a function of the conversion for all samples studied

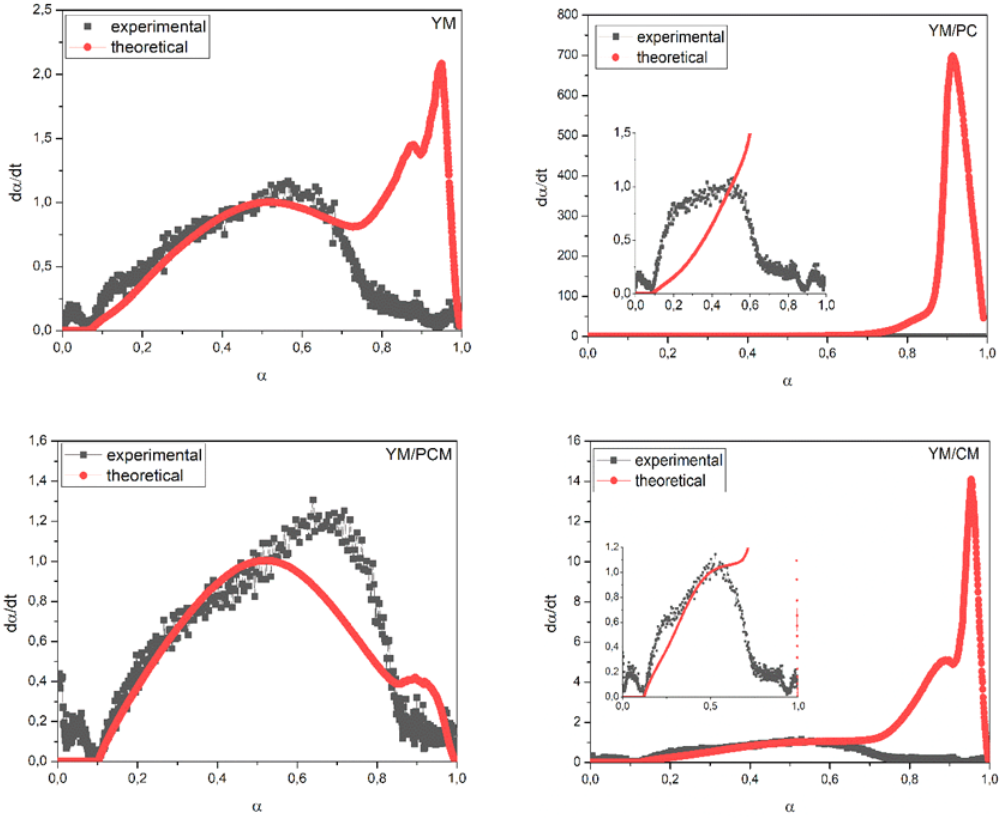

Figure 8: dα/dt vs conversion for all samples studied

According to Lopes and Tannous,[51] hemicelluloses decompose between $0.15 \leq \alpha \leq 0.45$, and cellulose – between $0.50 \leq \alpha \leq 0.90$. This can be demonstrated by the lower values of E_a provided in Table 4, as the cellulose is formed by very stable links, and therefore requires more energy for the decomposition of the chains. Thus, it is observed that the chemical (bleaching and TEMPO-mediated oxidation) and physical (steam explosion) treatments used to obtain the CNFs helped to remove the lignin and hemicelluloses, and increase thermal stability, which corroborates the FTIR analysis.

Aiming to determine possible changes in the step thermal degradation behavior, the approach proposed by Drozin *et al*. was used.[23] This approach compares the Vyazovkin and FWO methods over a selected temperature range, where a relative error >10% is indicative of a multi-step process. Hence, it is useful for rapid and easy identification of whether a treatment is effective for the removal of fibers, and its influence on the Arrhenius parameters. In this study, the entire temperature range was used. As reported by many authors, the main degradation is attributed to the cellulose,[54] as hemicelluloses make a great contribution to the early stages of cellulose degradation.[11] Lignin degrades over the whole temperature range.[55] Figure 7 presents E_a vs. α, whereas Figure 8 presents dα/dt vs. α for all the samples using both methods. The results for YM are: $E_{aVyazovkin}$ = 80.85 kJ.mol^{-1}, E_{aFWO} = 99.87 kJ.mol^{-1}, A = 0, m = 0.1, n = 1.99, and p = 0, with a relative error of 16.4%. The results for YM/PC are: $E_{aVyazovkin}$ = 137.98 kJ.mol^{-1}, E_{aFWO} = 156.16 kJ.mol^{-1}, A = 233.52 x 10^{-10}, m = 0.1, n = 1.99, and p = 0, with a relative error of 48.8%. The results for YM/PCM are: $E_{aVyazovkin}$ = 105.27 kJ.mol^{-1}, E_{aFWO} = 124.71 kJ.mol^{-1}, A = 0.05 x 10^{10}, m = 0.1, n = 1.99, and p = 0, with a relative error of 7.94%. The results for YM/CM are: $E_{aVyazovkin}$ = 110.21 kJ.mol^{-1}, E_{aFWO} = 129.15 kJ.mol^{-1}, A = 0.44 x 10^{10}, m = 0.1, n = 1.99, and p = 0, with a relative error of 14.8%. In addition, it can be observed that the suggested range of α = 0.2–0.8 is where the experimental and theoretical values are in proximity (Fig. 7).

Since no p value was observed from Equation 8 for all specimens, the probable reaction mechanism is diffusional (see Table 2). YM/PC is the only sample presenting a relative error lower than 10%, indicating a single-step stage process. YM, YM/PCM, and YM/CM present higher relative error values, indicating a multi-step stage process.

CONCLUSION

In this study, we verified the effects of different sequences of treatments conducted on samples of YM residues to evaluate the characteristics of the obtained CNFs. With the chemical (bleaching and TEMPO-oxidation) and physical (steam explosion) treatments, it was possible to partially remove the hemicelluloses and lignin. The treatments performed on the samples proved to be efficient in the delignification process to obtain the CNFs; this was verified from the FTIR spectra, which showed partial removal of the hemicelluloses and lignin. The treated samples showed greater initial thermal resistance than the YM fiber, and the YM/PCM sample showed the highest thermal stability – approximately 10% higher than that of the untreated sample. The higher thermal stability observed for the CNFs relative to that of the YM sample was also attributed to the higher Ea observed. The sample with the highest Ea was YM/PC, which was the sample that underwent physical (steam explosion) and chemical (bleaching and TEMPO-mediated oxidation) treatments to obtain the CNFs. The TEM micrographs corroborated the other characterizations, demonstrating the isolation of nanocellulose in all of the treated samples, and indicating that the physical, chemical, and mechanical treatments were efficient in obtaining CNFs. Thus, owing to the similar dimensions and morphologies of the obtained CNFs, the use of steam explosion, bleaching and ultra-fine grinding represents an adequate method for obtaining nanocellulose, using fewer chemical reagents and, therefore, generating less pollution, for achieving greater thermal stability and nanometric scale products.

ACKNOWLEDGEMENT: The authors thank Universidade do Vale do Taquari Univates and Universidade de Caxias do Sul (UCS) for supporting this research, and and Elacy for donating the residues of YM.

REFERENCES

1 D. Trache, A. F. Tarchoun, M. Derradji, T. S. Hamidon, N. Masruchin *et al*., *Front. Chem*., **8**, 392 (2020), https://doi.org/10.3389/fchem.2020.00392

2 P. Nehra and R. P. Chauhan, *Iran. Polym. J*., **31**,

771 (2022), https://doi.org/10.1007/s13726-022-01040-0
[3] P. Ligero, A. De Veja and X. Garcia, *Cellulose Chem. Technol.*, **57**, 49 (2023), https://doi.org/10.35812/CelluloseChemTechnol.2023.57.05
[4] M. A. Dahlem Jr., C. Borsoi, B. Hansen and A. L. Catto, *Carbohyd. Polym.*, **218**, 78 (2019), https://doi.org/10.1016/j.carbpol.2019.04.064
[5] M. P. Arrieta, L. Peponi, D. López and M. Fernández-García, *Ind. Crop. Prod.*, **111**, 317 (2018), https://doi.org/10.1016/j.indcrop.2017.10.042
[6] B. Hansen, C. Borsoi, M. A. Dahlem Jr. and A. L. Catto, *Ind. Crop. Prod.*, **140**, 111696 (2019), https://doi.org/10.1016/j.indcrop.2019.111696
[7] M. Gonçalves, M. C. Guerreiro, M. L. Bianchi, L. Carlos, A. Oliveira *et al.*, *Ciênc. Agrotec. Lavras.*, **31**, 1386 (2007)
[8] R. H. F. Faradilla, G. Lee, A. Rawal, T. Hutomo, M. H. Stenzel *et al.*, *Cellulose*, **23**, 3023 (2016), https://doi.org/10.1007/s10570-016-1025-8
[9] M. Y. Khalid, A. Al Rashid, Z. U. Arif, W. Ahmed and H. Arshad, *J. Mater. Res. Technol.*, **14**, 2601 (2021), https://doi.org/10.1016/j.jmrt.2021.07.128
[10] H. C. Chen, W. T. Y. Tze and F. C. Chang, *Cellulose*, **27**, 5757 (2020), https://doi.org/10.1007/s10570-020-03190-x
[11] R. M. Neves, H. L. Ornaghi, F. G. Ornaghi, S. C. Amico and A. J. Zattera, *J. Therm. Anal. Calorim.*, **147**, 879 (2022), https://doi.org/10.1007/s10973-020-10316-7
[12] A. Leszczyńska, P. Radzik, K. Haraźna and K. Pielichowski, *Thermochim. Acta*, **663**, 145 (2018), https://doi.org/10.1016/j.tca.2018.03.015
[13] H. P. S. Abdul Khalil, Y. Davoudpour, C. K. Saurabh, M. S. Hossain, A. S. Adnan *et al.*, *Renew. Sustain. Energ. Rev.*, **64**, 823 (2016), https://doi.org/10.1016/j.rser.2016.06.072
[14] H. Xie, H. Du, X. Yang and C. Si, *Int. J. Polym. Sci.*, **2018**, 7923068 (2018), https://doi.org/10.1155/2018/7923068
[15] M. S. Islam, N. Kao, S. N. Bhattacharya, R. Gupta and H. J. Choi, *Chinese J. Chem. Eng.*, **26**, 465 (2018), https://doi.org/10.1016/j.cjche.2017.07.004
[16] Y. Zhang, Q. Cheng, C. Chang and L. Zhang, *J. Appl. Polym. Sci.*, **135**, 1 (2018), https://doi.org/10.1002/app.46279
[17] Y. Nakamura, Y. Ono, T. Saito and A. Isogai, *Cellulose*, **26**, 6529 (2019), https://doi.org/10.1007/s10570-019-02560-4
[18] H. Yang, Y. Zhang, R. Kato and S. J. Rowan, *Carbohyd. Polym.*, **212**, 30 (2019), https://doi.org/10.1016/j.carbpol.2019.02.008
[19] D. Dallé, B. Hansen, A. J. Zattera, E. L. Francisquetti, A. L. Catto *et al.*, *Cellulose*, **28**, 2053 (2021), https://doi.org/10.1007/s10570-020-03657-x
[20] F. Meng, G. Wang, X. Du, Z. Wang, S. Xu *et al.*, *Compos. Part B Eng.*, **160**, 341 (2019), https://doi.org/10.1016/j.compositesb.2018.08.048
[21] J. Šesták and G. Berggren, *Thermochim. Acta*, **3**, 1 (1971), https://doi.org/10.1016/0040-6031(71)85051-7
[22] S. Vyazovkin, A. K. Burnham, J. M. Criado, L. A. Pérez-Maqueda, C. Popescu *et al.*, *Thermochim. Acta*, **520**, 1 (2011), https://doi.org/10.1016/j.tca.2011.03.034
[23] D. Drozin, S. Sozykin, N. Ivanova, T. Olenchikova, T. Krupnova *et al.*, *SoftwareX*, **11**, 100359 (2020), https://doi.org/10.1016/j.softx.2019.100359
[24] R. E. Gemmer, C. Borsoi, B. Hansen, M. A. Dahlem Jr., E. L. Francisquetti *et al.*, *J. Nat. Fibers*, **19**, 10539 (2022), https://doi.org/10.1080/15440478.2021.1994095
[25] V. R. Franceschi and P. A. Nakata, *Ann. Rev. Plant Biol.*, **56**, 41 (2005), https://doi.org/10.1146/annurev.arplant.56.032604.144106
[26] E. Kaffashsaie, H. Yousefi, T. Nishino, T. Matsumoto, M. Mashkour *et al.*, *Carbohyd. Polym.*, **262**, 117938 (2021), https://doi.org/10.1016/j.carbpol.2021.117938
[27] X. Zhao, F. Cheng and Y. Hu, *Fibers Polym.*, **22**, 59 (2021), https://doi.org/10.1007/s12221-021-0196-6
[28] H. Xiao, F. Yang, Q. Lin, Q. Zhang, W. Tang *et al.*, *Int. J. Biol. Macromol.*, **138**, 556 (2019), https://doi.org/10.1016/j.ijbiomac.2019.07.121
[29] D. J. Mendoza, C. Browne, V. S. Raghuwanshi, G. P. Simon and G. Garnier, *Carbohyd. Polym.*, **226**, 115292 (2019), https://doi.org/10.1016/j.carbpol.2019.115292
[30] H. Zergane, S. Abdi, H. Xu, J. Hemming, X. Wang *et al.*, *Ind. Crop. Prod.*, **144**, 112044 (2020), https://doi.org/10.1016/j.indcrop.2019.112044
[31] H. Zhang, Q. Li, F. Peng, H. Guo, L. Xiong *et al.*, *Iran. Polym. J.*, **29**, 535 (2020), https://doi.org/10.1007/s13726-020-00817-5
[32] L. N. Hugen, A. de Amorim dos Santos, E. H. de Novais Miranda, L. E. Silva, G. H. D. Tonoli *et al.*, *Iran. Polym. J.*, **32**, 165 (2023), https://doi.org/10.1007/s13726-022-01115-y
[33] Y. H. Feng, T. Y. Cheng, W. G. Yang, P. T. Ma, H. Z. He *et al.*, *Ind. Crop. Prod.*, **111**, 285 (2018), https://doi.org/10.1016/j.indcrop.2017.10.041
[34] S. Rashid and H. Dutta, *Ind. Crop. Prod.*, **154**, 112627 (2020), https://doi.org/10.1016/j.indcrop.2020.112627
[35] E. M. Sitinjak, I. Masmur, Y. Sitanggang, R. S. Pratikha, F. Nainggolan, *et al.*, *Cellulose Chem. Technol.*, **57**, 369 (2023), https://doi.org/10.35812/CelluloseChemTechnol.2023.57.32
[36] X. Weng, M. Guo, F. Luo and Z. Chen, *Chem. Eng. J.*, **308**, 904 (2017), https://doi.org/10.1016/j.cej.2016.09.134

[37] N. Nordin, S. H. Othman, S. A. Rashid and R. K. Basha, *Food Hydrocoll*., **106**, 105884 (2020), https://doi.org/10.1016/j.foodhyd.2020.105884
[38] H. Zhang, Y. Chen, S. Wang, L. Ma, Y. Yu *et al*., *Carbohyd*. *Polym*., **238**, 116180 (2020), https://doi.org/10.1016/j.carbpol.2020.11618
[39] E. L. Varetti and C. R. Volponi, *Appl*. *Spectrosc*., **49**, 537 (1995), https://doi.org/10.1366/0003702953964228.
[40] R. H. F. Faradilla, G. Lee, J. Y. Arns, J. Roberts, P. Martens *et al*., *Carbohyd*. *Polym*., **174**, 1153 (2017), https://doi.org/10.1016/j.carbpol.2017.07.025.
[41] M. Poletto, H. L. Ornaghi Jr. and A. J. Zattera, *Materials*, **7**, 6105 (2014), https://doi.org/10.3390/ma7096105
[42] S. Nam, A. D. French, B. D. Condon and M. Concha, *Carbohyd*. *Polym*., **135**, 1 (2016), https://doi.org/10.1016/j.carbpol.2015.08.035
[43] M. Asim, M. T. Paridah, M. Chandrasekar, R. M. Shahroze, M. Jawaid *et al*., *Iran*. *Polym*. *J*., **29**, 625 (2020), https://doi.org/10.1007/s13726-020-00824-6
[44] J. Y. Yeo, B. L. F. Chin, J. K. Tan and Y. S. Loh, *J*. *Energ*. *Inst*., **92**, 27 (2019), https://doi.org/10.1016/j.joei.2017.12.003
[45] H. Fukuzumi, T. Saito, T. Iwata, Y. Kumamoto and A. Isogai, *Biomacromolecules*, **10**, 162 (2009), https://doi.org/10.1021/bm801065u
[46] H. Fukuzumi, T. Saito, Y. Okita and A. Isogai, *Polym*. *Degrad*. *Stab*., **95**, 1502 (2010), https://doi.org/10.1016/j.polymdegradstab.2010.06.015
[47] K. Singh, M. Risse, K. C. Das and J. Worley, *J*. *Energ*. *Resour*. *Technol*. *Trans*., **131**, 0222011 (2009), https://doi.org/10.1115/1.3120349
[48] M. Yahya, Y. W. Chen, H. V. Lee, C. C. Hock and W. H. W. Hassan, *J*. *Polym*. *Environ*., **27**, 678 (2019), https://doi.org/10.1007/s10924-019-01373-7
[49] D. Ahuja, L. Kumar and A. Kaushik, *Carbohyd*. *Polym*., **255**, 117466 (2021), https://doi.org/10.1016/j.carbpol.2020.117466
[50] H. L. Ornaghi, F. G. Ornaghi, R. M. Neves, F. Monticeli and O. Bianchi, *Cellulose*, **27**, 4949 (2020), https://doi.org/10.1007/s10570-020-03132-7
[51] F. C. R. Lopes and K. Tannous, *Thermochim*. *Acta*, **691**, 178714 (2020), https://doi.org/10.1016/j.tca.2020.178714
[52] C. Borsoi, M. A. Dahlem Júnior, L. V. R. Beltrami, B. Hansen, A. J. Zattera *et al*., *J*. *Therm*. *Anal*. *Calorim*., **139**, 3275 (2020), https://doi.org/10.1007/s10973-019-08666-y
[53] F. X. Xu, X. Zhang, F. Zhang, L. Q. Jiang, Z. L. Zhao *et al*., *Fuel*, **268**, 117365 (2020), https://doi.org/10.1016/j.fuel.2020.117365
[54] H. L. Ornaghi, F. G. Ornaghi, K. C. C. de Carvalho Benini and O. Bianchi, *Cellulose*, **26**, 7145 (2019), https://doi.org/10.1007/s10570-019-02610-x
[55] J. Gassan and A. K. Bledzki, *J*. *Appl*. *Polym*. *Sci*., **82**, 1417 (2001), https://doi.org/10.1002/app.1979